Comparison of simplified Monte Carlo simulation and diffusion approximation for the fluorescence signal from phantoms with typical mouse tissue optical properties

Guobin Ma, Jean-François Delorme, Pascal Gallant, and David A. Boas

A simplified approach is proposed to simulate the fluorescence signal from a fluorophore submerged inside a turbid medium using the Monte Carlo method. Based on the reversibility of photon propagation, the fluorescence signal can be obtained from a single Monte Carlo simulation of the excitation light. This is computationally less expensive and also allows for the direct use of well-validated nonfluorescence photon migration Monte Carlo codes. Fluorescence signals from a mouse tissuelike phantom were computed using both the simplified Monte Carlo simulation and the diffusion approximation. The relative difference of signal intensity was found to be at most 30% for a fluorophore placed in the medium at various depths and horizontally midway between a source–detector pair separated by 3 mm. The difference in time characteristics of the signal is also examined. © 2007 Optical Society of America

OCIS codes: 170.3660, 170.6280, 170.5280, 290.1990, 170.7050.

1. Introduction

Light propagation in strongly scattering tissue has been extensively studied in the past few decades in response to an expanding interest in applications of optical imaging for biomedical diagnostic and therapeutic use. Fluorescence techniques represent an important class of optical methods being applied to *in vitro* and *in vivo* biomedical diagnostics, including noninvasive molecular sensing and imaging.[1–8] Measured tissue fluorescence signals reflect both intrinsic tissue pathology (local morphological, biochemical, and optical properties), as well as experimental design features (including excitation and emission wavelengths, fiber-optic probe design, and contrast agent concentration). Model-based computations are often employed to quantitatively simulate photon migration characteristics in tissues, thereby enabling accurate analysis and interpretation of measured tissue-fluorescence signals.

Photon propagation in biological tissue is governed by the radiative transfer equation (RTE) in which light is considered to be composed of neutral particles.[9–11] However, use of the RTE is computationally expensive in practical biomedical imaging. Alternative stochastic approaches can be used to model photon transport in turbid media. Monte Carlo (MC) modeling was first applied to study light dosimetry in tissues in 1983 (Ref. 12) and has been shown to provide the most accurate results in comparison with experiment.[13–15] Similarly, MC simulations of heterogeneous tissue models based on magnetic resonance imaging (MRI)[16] and computed tomography (CT)[17] results have been explored, although computation is heavier. Some researchers have also examined the temporal and spectral characteristics of fluorescence in tissue with the MC method.[18] A common simplification to these approaches is the diffusion approximation (DA), which yields analytical solutions for the light energy distribution when applied to simple geometries.[19–22] The applicable conditions of the DA are[19]: photon scattering dominates over absorption, and the point of interest is far from source or boundaries. In the near-infrared (NIR) spectral range, the optical absorption of tissue is much smaller than scattering. As a result, it is well-established that the DA provides an accurate description of NIR light distribution in tissue[9,10,14,16,19,20] both for optical tomography[10,16,23]

G. Ma (gma@art.ca), J.-F. Delorme, and P. Gallant are with Advanced Research Technologies, Incorporated (ART), 2300 Alfred-Nobel Boulevard, St.-Laurent, Quebec H4S 2A4, Canada. D. A. Boas is with the Athinoula A. Martinos Center for Biomedical Imaging, Massachusetts General Hospital, Harvard Medical School, Charlestown, Massachusetts 02129.

and fluorescence imaging[6–8] if applied to bulk tissue in regions several transport mean-free-path lengths away from the source. Therefore, fluorophore location and concentration can be quickly estimated[24] from the measured time-resolved fluorescence signal using the analytical solution of the DA. However, several concerns exist about the validity of the DA, notably, its applicability in small tissue volumes as well as its accuracy without prior knowledge of tissue optical properties and the heterogeneous features and irregular shape of a mouse body. This study is limited to the validity of the DA as applied to small animals. It is examined by comparing the fluorescence signal from a commercial small animal imager[25] (eXploreOptix, ART, St. Laurent, Quebec, Canada) predicted by the MC and DA methods. Other issues either have already been studied elsewhere,[26] or will be addressed later in our ongoing studies.

In the following, we first briefly describe a model to compute the fluorescence signal from turbid medium using the DA. Then, a simplified method based on MC simulation to compute the fluorescence signal from diffusive medium is introduced. Based on the reversibility of light propagation, the fluorescent photon flux is obtained directly from a single MC simulation of the excitation light. In this way, computation time can be reduced by orders of magnitude. Later, the simplified MC results will be used as the reference to examine the fluorescence signal predicted by the DA for a tissuelike phantom in order to estimate the error range of the DA model specifically for the hardware configuration of eXplore Optix and typical tissue optical properties of small animals. The upper limit of the error was found to be ~30% and existed only in some specific regions (shallow fluorophore depths).

2. Model Description

To simulate the fluorescence generated from a fluorophore inside a turbid medium such as tissue, light transport in the medium must be accounted for. In general, the detected fluorescence signal $F(\vec{r}, t)$ from a point fluorophore is a convolution of the following[27,28]:

$$
\begin{aligned}
F(\vec{r}, t) &= \int \int \int H_x(\vec{r} - \vec{r}_s, t''') \left[\sum_i \frac{A_i}{\tau_i} \exp\left(-\frac{t'' - t'''}{\tau_i} \right) \right] \\
&\quad \times E_m(\vec{r}_d - \vec{r}, t' - t'') S(t - t') dt' dt'' dt''' \\
&= H_x(\vec{r} - \vec{r}_s, t) \otimes \left[\sum_i \frac{A_i}{\tau_i} \exp\left(-\frac{t}{\tau_i} \right) \right] \\
&\quad \otimes E_m(\vec{r}_d - \vec{r}, t) \otimes S(t),
\end{aligned} \tag{1}
$$

where the $\otimes$ sign represents the convolution integral, $H_x(\vec{r} - \vec{r}_s, t)$ is the light propagated from the excitation source at position $\vec{r}_s$ to the fluorophore at $\vec{r}$, $E_m(\vec{r}_d - \vec{r}, t)$ is the fluorescent light propagated from the fluorophore at $\vec{r}$ to the detector at $\vec{r}_d$. $S(t)$ is the system impulse response function (IRF). The terms in square brackets represent fluorescent decay

after excitation, where A_i and τ_i are the amplitude and lifetime of the ith fluorophore component. A_i is usually related to the concentration, extinction coefficient, and quantum yield of the fluorophore. Since this study focuses on the issue of light propagation in tissue, which is described by $H_x(\vec{r} - \vec{r}_s, t)$ and $E_m(\vec{r}_d - \vec{r}, t)$, it is convenient to take out the terms not related to photon propagation. In other words, we simply assume that

$$
\left[\sum_i \frac{A_i}{\tau_i} \exp\left(-\frac{t}{\tau_i} \right) \right] \otimes S(t) = 1,
$$

and the quantity we are examining is

$$
F_0(\vec{r}, t) = H_x(\vec{r} - \vec{r}_s, t) \otimes E_m(\vec{r}_d - \vec{r}, t). \tag{2}
$$

This corresponds to instant fluorescence lifetime and system IRF. Here we compare $F_0(\vec{r}, t)$ when $H_x(\vec{r} - \vec{r}_s, t)$ and $E_m(\vec{r}_d - \vec{r}, t)$ are obtained by the DA and the simplified fluorescent MC simulation. In practice, fluorescence lifetime and system IRF are always finite. To adapt that, the results presented here can be generalized by convolving with the fluorescent decay and the system IRF terms[27]

$$
F(\vec{r}, t) = F_0(\vec{r}, t) \otimes \left[\sum_i \frac{A_i}{\tau_i} \exp\left(-\frac{t}{\tau_i} \right) \right] \otimes S(t). \tag{3}
$$

Because the fluorescent decay and the system IRF are independent of photon propagation in tissue, the convolutions in Eq. (3) will not affect the conclusion regarding the DA and the MC. This aspect will not be discussed further in this paper.

A. Configuration Geometry

Our computations are based on the reflection geometry used in eXplore Optix that is illustrated in Fig. 1. Both the excitation light source and the detector are on the surface of the medium while the fluorophore can be anywhere inside. Excitation laser photons are injected perpendicularly to the phantom surface, and fluorescent emission is detected at a position $\rho = 3$ mm away from the source. All the results presented here were obtained with this configuration, unless specified and are based on the following: a Cartesian coordinate system was used in the computation, the location of the excitation source was chosen as the
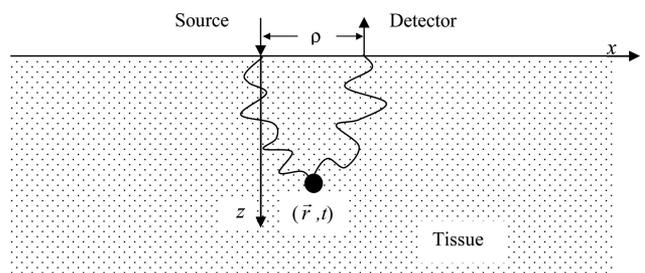

Fig. 1. Schematic of fluorescence spectroscopy in turbid medium such as biological tissue when reflection geometry is used.

origin, the x–y plane was coincident with the medium surface, the x axis was from the source to the detector, and the z axis was perpendicular to the medium surface and pointing to the medium.

B. Diffusion Approximation

The solution of the photon diffusion equation for a homogeneous slab medium for a time-domain measurement with an impulse point source of light is given by[19–22]

$$\Phi(x, y, z, t) = \frac{v \exp\left(-\mu_a v t - \frac{x^2 + y^2}{4Dvt}\right)}{4\pi(4\pi Dvt)^{3/2}}$$
$$\times \left\{ \sum_{m=-\infty}^{m=+\infty} \exp\left[-\frac{(z - z_{+,m})^2}{4Dvt} \right] \right.$$
$$\left. - \sum_{m=-\infty}^{m=+\infty} \exp\left[-\frac{(z - z_{-,m})^2}{4Dvt} \right] \right\}, \quad (4)$$

where $\Phi(x, y, z, t)$ is the photon fluence at position $\vec{r} = (x, y, z)$ and time t, generated by a point source of unitary amplitude at position $(0, 0, 0)$; $D = v/(3\mu_s')$ is the photon diffusion coefficient; μ_s' is the reduced scattering coefficient; μ_a is the absorption coefficient; and v is the speed of light in the medium. To satisfy the extrapolated boundary condition,[21] the method of images[19,20,22] is used. The positions of the image sources are at $(0, 0, z_{+,m})$ and $(0, 0, z_{-,m})$ with

$$z_{+,m} = 2m(s + 2z_b) + z_0,$$
$$z_{-,m} = 2m(s + 2z_b) - 2z_b - z_0, \quad (5)$$

where s is the slab thickness, $z_b = (1 + R_{eff})/(1 - R_{eff})2D$ is the distance between the medium surface and the extrapolated boundary where the photon fluence equals zero, and R_{eff} is the internal reflectance due to refractive index mismatch between the air and the medium. R_{eff} can be approximated to a simple equation[29]:

$$R_{eff} = -1.440n^{-2} + 0.710n^{-1} + 0.668 + 0.0636n \quad (6)$$

for relative refractive index $n = n_{\text{tissue}}/n_{\text{air}}$ with an error less than 10% compared with its exact value computed using Fresnel reflection coefficient. Alternatively, z_b can be calculated with more complicated formulas for better precision.[22] To model high directional beam (e.g., laser) by DA, an isotropic source located at $z_0 = 1/\mu_s'$ is assumed. That is the origin of z_0 in Eqs. (5).

When the DA solution is applied to our case, $\Phi(x, y, z, t)$ is the photon propagation Green's function of excitation light $H_x(\vec{r} - \vec{r}_s, t)$ with $\vec{r}_s = 0$. Now $E_m(\vec{r}_d - \vec{r}, t)$ must be calculated. From the process by which $\Phi(x, y, z, t)$ is obtained, it can be found that $\Phi(x, y, z, t)$ is the photon fluence at $\vec{r} = (x, y, z)$ for an isotropic source located at $\vec{r}_s = (0, 0, z_0)$. The photon propagation Green's function of fluorescence light

$E_m(\vec{r}_d - \vec{r}, t)$ can be obtained similarly. Indeed, the photon fluence at $\vec{r}_d = (x_d, y_d, z_d)$ from an isotropic source at the fluorophore location $\vec{r} = (x, y, z)$ has the same form of Eq. (4) when $\vec{r} = (x, y, z)$ is replaced by $\vec{r}_d = (x_d, y_d, z_d)$, and $\vec{r}_s = (0, 0, z_0)$ is replaced by $\vec{r} = (x, y, z)$. Explicitly, it can be written as

$$E_m(\vec{r}_d - \vec{r}, t) = \frac{v \exp\left(-\mu_a v t - \frac{(x_d - x)^2 + (y_d - y)^2}{4Dvt}\right)}{4\pi(4\pi Dvt)^{3/2}}$$
$$\times \left\{ \sum_{m=-\infty}^{m=+\infty} \exp\left[-\frac{(z_d - z_{+,m}{}^{em})^2}{4Dvt} \right] \right.$$
$$\left. - \sum_{m=-\infty}^{m=+\infty} \exp\left[-\frac{(z_d - z_{-,m}{}^{em})^2}{4Dvt} \right] \right\}, \quad (7)$$

where

$$z_{+,m}{}^{em} = 2m(s + 2z_b) + z,$$
$$z_{-,m}{}^{em} = 2m(s + 2z_b) - 2z_b - z \quad (8)$$

are the positions of the image sources to ensure that the photon fluence equals zero at extrapolated boundary z_b. Also, diffusion coefficient D and absorption coefficient μ_a for fluorescent photons are assumed to be the same as that of excitation photons.

C. Monte Carlo Simulation

Detailed descriptions of the MC simulation of photon migration in tissue can be found elsewhere.[14–18] In short, it generates a statistical distribution of photons absorbed by each voxel in tissue by following the trajectory of a large number of photons. Many measurable quantities can be deduced from this distribution. In our simulation, the well-validated MC codes MCML[14] and tMCimg[16] are used. MCML is straightforward but only gives cw results for a layered tissue structure. To conduct time-resolved simulations, tMCimg is required. In addition, tMCimg has more flexibility to count for the 3D heterogeneous tissue properties.

The scenario of photon propagation in nonfluorescent tissue is that photons are launched at the source location—some are absorbed, some are scattered—and only a portion of them will reach the detector. Fluorescence in tissue can be treated as a two-step process, similar to the diffusion approach described earlier, if instant fluorescent lifetime is assumed. The fluorophore acts like a detector to receive excitation photons in the first step and a source to emit fluorescent photons in the second step. In the well-established traditional MC simulation, the statistical distribution of photons absorbed in each voxel is computed, which can be converted to photon fluence by dividing it by the absorption coefficient μ_a. This is the first step of fluorescence, corresponding to the calculation of $H_x(\vec{r} - \vec{r}_s, t)$ under DA. Then the photons absorbed at $\vec{r}$ are converted to fluorescence and their propagation is simulated in a similar manner as for the first step.

This is equivalent to computing $E_m(\vec{r}_d - \vec{r}, t)$ under DA. Due to light attenuation, the number of photons that reach position $\vec{r}$ decreases exponentially with the distance relative to the position of the light source $|\vec{r} - \vec{r}_s|$. To obtain meaningful statistics and a good signal-to-noise ratio at the detector, many more photons are required for fluorescence MC simulation compared with the nonfluorescence one. As a result, the computation load is much heavier.

A simplified method for fluorescence MC simulation is introduced here. Suppose A and B are two locations in a medium. The probability to detect a photon at A when it is injected at B is the same as that to detect it at B if it is injected at A thanks to the reversibility of photon propagation in the medium. This statement is still true even if the medium between A and B is not continuous, for example, when a photon passes the interface of two types of medium. Indeed, the photon behavior at the interface of different media in MC simulation is described by the classical Fresnel equation.[14,16] Based on this fact, it is possible to assume that the probability to detect a photon at $\vec{r}$ when it is launched at the source position $\vec{r}_s$ is the same as the probability to detect it at $\vec{r}_s$ if it is injected at $\vec{r}$. Applying this principle to the second step of fluorescent MC simulation, we can simply use the results from the first step if the difference in optical properties due to excitation and emission wavelengths is ignored. In most cases, the difference in optical properties in the wavelength range of excitation and emission is small enough to be negligible. Therefore, the probability to detect a fluorescence photon at the position of excitation source is the same as the probability to detect an excitation photon at the fluorophore location. Furthermore, we can use the results of MC simulation for excitation light $H_x(\vec{r} - \vec{r}_s, t)$ to represent the fluorescent light propagation for a detector at any position $E_m(\vec{r}_d - \vec{r}, t)$ as long as the following two conditions are satisfied: the optical characteristics of the media between source to fluorophore and fluorophore to detector are identical and the distances from source to fluorophore and from fluorophore to detector are the same.

Specifically to the configuration shown in Fig. 1, the excitation photons are injected at $\vec{r}_s = (0, 0, 0)$, and the detector is at $\vec{r}_d = (3, 0, 0)$. The photon fluence of excitation light $H_x(\vec{r} - \vec{r}_s, t)$ at $\vec{r} = (x, y, z)$ is first computed by the nonfluorescence MC simulation. The photon fluence $E_m(\vec{r}_d - \vec{r}, t)$ detected at $\vec{r}_d$ for the fluorescent signal coming from $\vec{r}$ is the same as the excitation photon fluence $H_x(\vec{r} - \vec{r}_d, t)$ at $\vec{r}$ when injected at $\vec{r}_d$. Since the medium is a homogeneous slab, the distribution of excitation photons for the source at $\vec{r}_d = (3, 0, 0)$ can be obtained from that of the source at $\vec{r}_s = (0, 0, 0)$ by shifting the coordinates only 3 mm along the x axis. In this way, the measurable fluorescent signal can be calculated from a single MC simulation of the excitation light. In addition to directly using the nonfluorescence MC codes for fluorescence simulation, the computation time is greatly reduced.

D. Phantom Properties

The results presented below were obtained with a homogeneous tissuelike slab phantom with a thickness of 18 mm. For MCML, the slab is infinitely wide. For tMCimg, the phantom dimensions in the x and y directions are both 50 mm. Its optical properties are absorption coefficient $\mu_a = 0.03$ mm^{-1}, scattering coefficient $\mu_s = 10$ mm^{-1}, asymmetry factor of scattering function $g = 0.9$, and refractive index $n = 1.4$. These are all typical values for mouse tissue in the NIR spectral region.[30–32]

3. Results and Discussion

We first compare the fluorescence signal intensity computed by the MC and the DA. To begin, $H_x(\vec{r} - \vec{r}_s, t)$ and $E_m(\vec{r}_d - \vec{r}, t)$ are calculated by the DA [Eqs. (4) and (7)]. Meanwhile they can be computed by the simplified MC (MCML[14]) method described above. Then the fluorescence intensities $F_0(\vec{r}, t)$ by the DA and the MC are calculated according to Eq. (2) for a point fluorophore placed only in a single voxel at position $\vec{r} = (x, y, z)$ inside the medium. Shown in Fig. 2 is a contour plot of the logarithm of the fluorescence intensities calculated by the DA and the MC in the x–z plane at $y = 0$, corresponding to the configuration shown in Fig. 1, i.e., the excitation source at $(0, 0, 0)$, detector at $(3, 0, 0)$, and fluorophore at various positions $(x, 0, z)$. When a fluorophore is located away from the source and detector, the DA result is very close to the MC simulation, as expected. This, from one aspect, validates the simplified method of fluorescence MC simulation, based on the fact that the DA describes well the photon propagation in regions away from source and detector in scattering dominated medium. However, we are more interested in the regions close to the source and/or the detector,
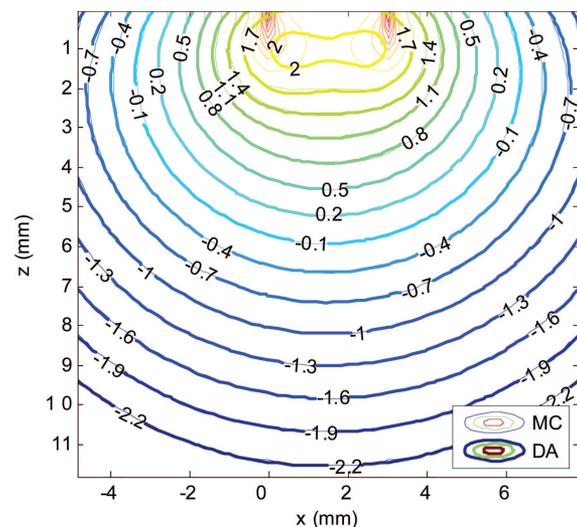

Fig. 2. (Color online) Comparison of the fluorescent intensity reaches the detector at $(3, 0, 0)$ for a point fluorophore placed in a single pixel at various positions (x, z) in the x–z plane excited by a unitary impulse light source injected at $(0, 0, 0)$ calculated by the simplified MC and the DA for the configuration geometry shown in Fig. 1.
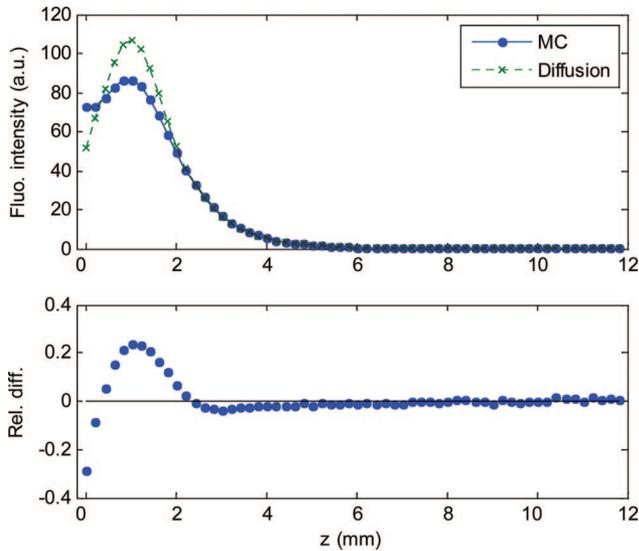
Fig. 3. (Color online) Fluorescence intensity calculated by the MC and the DA (upper panel) and the relative difference of the MC and the DA (lower panel) for a point fluorophore positioned horizontally midway between the source–detector pair at various depths inside the medium. The source–detector separation is 3 mm.
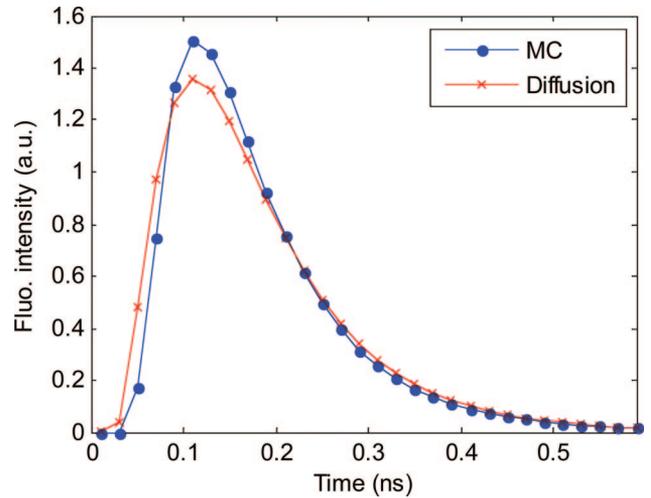

Fig. 4. (Color online) TPSF from a fluorescence signal calculated by the MC and the DA for a point fluorophore positioned horizontally midway between the source–detector pair at depth $z = 5.25$ mm inside the medium. The source–detector separation is 3 mm.

where significant differences exist between the DA and the MC. To quantify the difference, especially for the cases explored in Ref. 24, the fluorescence intensity calculated using the MC and the DA is shown in Fig. 3 for a fluorophore placed equidistantly on the x axis between the source and the detector (i.e., $x = 1.5$ mm, $y = 0$ mm) but at various depths z. The relative difference of the MC and the DA is plotted over z in the lower panel. One can see that as long as the fluorophore depth is larger than 3 mm, the relative difference is less than 4%. Even at a depth smaller than 3 mm, the largest difference is only ~30%.

One of the most important features of eXplore Optix is that it acquires time-resolved data that can be used to obtain quantitative information of the fluorophore. To explore the time characteristics of the fluorescent signal propagation in tissue, tMCimg[16] is employed for the same phantom described above. By applying the simplified MC method, the time-resolved fluorescence signal is calculated using Eq. (2) from a single MC simulation of the excitation light. The cw fluorescence intensities obtained by integrating the time-resolved signal (not shown here) are identical with the results from MCML for fluorophore at various positions. This confirms the consistency of the two MC codes. Shown in Figs. 4 and 5 are the time-related results. Figure 4 shows the comparison of a time point-spread function (TPSF) of fluorescence signal calculated by the MC and the DA for a point fluorophore positioned equidistantly between the source–detector pair ($x = 1.5$ mm, $y = 0$ mm) along the x axis at depth $z = 5.25$ mm inside the medium. The TPSF reflects the temporal characteristics of diffusion effect for light propagation in tissue. Here the calculations are done for impulse excitation light source and instant fluorescence life-

time. If there is no diffusion, the fluorescence signal reaching the detector should still be an impulse but with some delay. Due to diffusion, the impulse is spread. The extent of the spreading depends on the path length of a photon and the optical properties of the medium. Nevertheless, the location of a fluorophore can be estimated from the time position of the TPSF peak ($t_{TPSF\mathrm{max}}$).[24] For the TPSFs shown in Fig. 4, the time-integrated cw intensities by the DA and the MC are close (difference less than 4%, consistent with that shown in Fig. 3), although the shapes are slightly different. The time position of the TPSF peak is the same for the DA and the MC when a 20 ps time
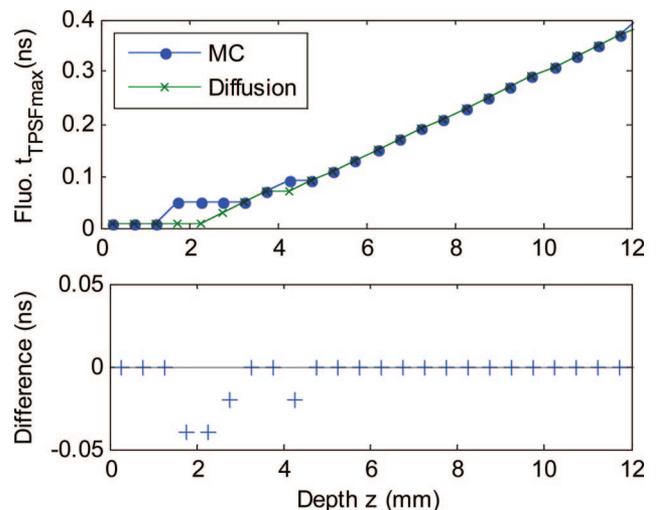

Fig. 5. (Color online) Time position of a fluorescence TPSF peak calculated by the MC and the DA (upper panel) and the difference of the MC and the DA (lower panel) for a point fluorophore positioned horizontally midway between the source–detector pair at various depths inside the medium. The source–detector separation is 3 mm.

step is used. In other words, the difference of $t_{TPSF\max}$ for a fluorophore at this depth is less than 20 ps. The $t_{TPSF\max}$ for a fluorophore at other depths for the same x (1.5 mm) and y (0 mm) positions are plotted in Fig. 5 together with the difference between the results by the DA and the MC simulation. It is evident that the DA closely matches the MC as long as the fluorophore depth is larger than 3 mm. Even for depths less than 3 mm, the maximum difference is less than 40 ps.

From these results it can be concluded that the DA is adequate for a quick estimation when processing the fluorescent signal from mouse tissue. Given its advantage of being an analytical solution that is fast to compute, the DA is preferable, especially when the time position of the fluorescent TPSF peak and fluorescence intensity are the main quantities used to extract fluorophore information in the medium, as described in Ref. 24. For *in vivo* experiments, of course, there are other error sources in addition to application of the DA. One is the validity of the homogeneity assumption, while the second is the use of slab geometry, and the third is the accuracy of the mouse tissue optical properties used. In practice, a small animal such as a mouse is neither a slab nor a cylinder and is also highly heterogeneous. In addition, every mouse differs both in shape and the optical properties of its tissue, which also change with physiological conditions. To precisely measure the optical properties of small animals *in situ* is another challenge. The impact of these issues is also under investigation and some of them have already been addressed by others.[26]

In summary, we introduced a simplified MC method to simulate the fluorescence signal from a fluorophore inside a turbid medium, such as tissue, based on the reversibility of photon propagation. The new method directly utilizes well-validated nonfluorescence MC codes and can save a lot of computation time. It can be used to compute fluorescence signal from tissues in most applications as long as the specified conditions are satisfied. One of the conditions is the assumption that the medium optical properties are identical for fluorescence excitation and emission photons. Actually, this limitation can be removed by scaling the MC results for excitation photons to emission ones using the perturbation MC method.[33,34]

Also, by comparing the results from the diffusion approximation with MC simulation, we found that the diffusion approximation is not a significant issue when it is used to interpret the fluorescence signal from mouse tissue. Large errors are found only when applying the DA at shallow depths, which are at most 30% for the cases examined in this paper. Otherwise the DA provides a computationally fast approach to calculate the fluorescence signal that can potentially be extended to account for inhomogeneity and irregular shape of mouse tissues using its numerical solution based on finite-element mesh.

References

1. M. A. O'Leary, D. A. Boas, X. D. Li, B. Chance, and A. G. Yodh, "Fluorescence lifetime imaging in turbid media," Opt. Lett. **21,** 158–160 (1996).
2. B. B. Das, F. Liu, and R. R. Alfano, "Time-resolved fluorescence and photon migration studies in biomedical and model random media," Rep. Prog. Phys. **60,** 227–292 (1997).
3. J. Chang, H. L. Graber, and R. L. Barbour, "Imaging of fluorescence in highly scattering media," IEEE Trans. Biomed. Eng. **44,** 810–822 (1997).
4. H. B. Jiang, "Frequency-domain fluorescent diffusion tomography: a finite-element-based algorithm and simulations," Appl. Opt. **37,** 5337–5343 (1998).
5. M. J. Eppstein, D. E. Dougherty, T. L. Troy, and E. M. Sevick-Muraca, "Biomedical optical tomography using dynamic parameterization and Bayesian conditioning on photon migration measurements," Appl. Opt. **38,** 2138–2150 (1999).
6. V. Ntziachristos and R. Weissleder, "Experimental three-dimensional fluorescence reconstruction of diffuse media using a normalized Born approximation," Opt. Lett. **26,** 893–895 (2001).
7. V. Ntziachristos, C. Tung, C. Bremer, and R. Weissleder, "Fluorescence-mediated tomography resolves protease activity *in vivo*," Nat. Med. **8,** 757–760 (2002).
8. A. B. Milstein, S. Oh, K. J. Webb, C. A. Bouman, Q. Zhang, D. A. Boas, and R. P. Millane, "Fluorescence optical tomography," Appl. Opt. **42,** 3081–3094 (2003).
9. A. Ishimaru, "Diffusion of light in turbid material," Appl. Opt. **28,** 2210–2215 (1989).
10. S. R. Arridge, "Optical tomography in medical imaging," Inverse Probl. **15,** R41–R93 (1999).
11. A. D. Klose, V. Ntziachristos, and A. H. Hielscher, "The inverse source problem based on the radiative transfer equation in optical molecular imaging," J. Comput. Phys. **202,** 323–345 (2005).
12. B. C. Wilson and G. Adam, "A Monte Carlo model for the absorption and flux distribution of light in tissue," Med. Phys. **10,** 824–830 (1983).
13. G. Zaccanti, "Monte Carlo study of light propagation in optically thick media: point source case," Appl. Opt. **30,** 2031–2041 (1991).
14. L.-H. Wang, S. L. Jacques, and L.-Q. Zheng, "MCML—Monte Carlo modeling of photon transport in multilayered tissues," Comput. Methods Programs Biomed. **47,** 131–146 (1995).
15. K. Vishwanath, B. W. Pogue, and M.-A. Mycek, "Quantitative fluorescence lifetime spectroscopy in turbid media: comparison of theoretical, experimental and computational methods," Phys. Med. Biol. **47,** 3387–3405 (2002).
16. D. A. Boas, J. P. Culver, J. J. Stott, and A. K. Dunn, "Three-dimensional Monte Carlo code for photon migration through complex heterogeneous media including the adult human head," Opt. Express **10,** 159–170 (2002).
17. H. Li, J. Tian, F. P. Zhu, W. X. Cong, L. V. Wang, E. A. Hoffman, and G. Wang, "A mouse optical simulation environment (MOSE) to investigate bioluminescent phenomena with the Monte Carlo method," Acad. Radiol. **11,** 1029–1038 (2004).
18. K. Vishwanath and M. Mycek, "Time-resolved photon migration in bi-layered tissue models," Opt. Express **13,** 7466–7482 (2005).
19. M. S. Patterson, B. Chance, and B. Wilson, "Time resolved reflectance and transmittance for the noninvasive measurement of tissue optical properties," Appl. Opt. **28,** 2331–2336 (1989).
20. A. Kienle and M. S. Patterson, "Improved solutions of the steady-state and the time-resolved diffusion equations for reflectance from semi-infinite turbid medium," J. Opt. Soc. Am. A **14,** 246–254 (1997).
21. R. C. Haskell, L. O. Svaasand, T. Tsay, T. Feng, M. S. McAdams,

and B. J. Tromberg, "Boundary conditions for the diffusion equation in radiative transfer," J. Opt. Soc. Am. A **11,** 2727–2741 (1994).

22. D. Contini, F. Martelli, and G. Zaccanti, "Photon migration through a turbid slab described by a model based on diffusion approximation. I. Theory," Appl. Opt. **36,** 4587–4599 (1997).

23. E. Hillman, "Experimental and theoretical investigations of near infrared tomographic imaging methods and clinical applications," Ph.D. dissertation (University of London, 2002).

24. D. Hall, G. Ma, F. Lesage, and Y. Wang, "Simple time-domain optical method for estimating the depth and concentration of a fluorescent inclusion in a turbid medium," Opt. Lett. **29,** 2258–2260 (2004).

25. P. Gallant, A. Belenkov, G. Ma, F. Lesage, Y. Wang, D. Hall, and L. McIntosh, "A quantitative time-domain optical imager for small animals in vivo fluorescence studies," in *Biomedical Optics Topical Meeting* on CD-ROM (Optical Society of America, 2004), paper WD2.

26. A. Soubret, J. Ripoll, and V. Ntziachristos, "Accuracy of fluorescent tomography in the presence of heterogeneities: study of the normalized born ratio," IEEE Trans. Med. Imaging **24,** 1377–1386 (2005).

27. M. S. Patterson and B. Pogue, "Mathematical model for time-resolved and frequency-domain fluorescence spectroscopy in biological tissues," Appl. Opt. **33,** 1963–1974 (1994).

28. E. M. Sevick-Muraca and C. L. Burch, "Origin of phosphorescence signals reemitted from tissues," Opt. Lett. **19,** 1928–1930 (1994).

29. R. A. Groenhuis, H. A. Ferwerda, and J. J. ten Bosch, "Scattering and absorption of turbid materials determined from reflection measurements. 1. Theory," Appl. Opt. **22,** 2456–2462 (1983).

30. E. E. Graves, J. Ripoll, R. Weissleder, and V. Ntziachristos, "A submillimeter resolution fluorescence molecular imaging system for small animal imaging," Med. Phys. **30,** 901–911 (2003).

31. K. Ren, B. Moa-Anderson, G. Bal, X. Gu, and A. H. Hielscher, "Frequency domain tomography in small animals with the equation of radiative transfer," in *Optical Tomography and Spectroscopy of Tissue VI,* B. Chance, R. R. Alfano, B. J. Tromberg, M. Tamura, and E. M. Sevick-Muraca, eds., Proc. SPIE **5693,** 111–120 (2005).

32. G. Alexandrakis, F. R. Rannou, and A. F. Chatziioannou, "Tomographic bioluminescence imaging by use of a combined optical-PET (OPET) system: a computer simulation feasibility study," Phys. Med. Biol. **50,** 4225–4241 (2005).

33. C. K. Hayakawa, J. Spanier, F. Bevilacqua, A. K. Dunn, J. S. You, B. J. Tromberg, and V. Venugopalan, "Perturbation Monte Carlo methods to solve inverse photon migration problems in heterogeneous tissues," Opt. Lett. **26,** 1335–1337 (2001).

34. Y. Phaneendra Kumar and R. M. Vasu, "Reconstruction of optical properties of low-scattering tissue using derivative estimated through perturbation Monte-Carlo method," J. Biomed. Opt. **9,** 1002–1012 (2004).